ChemComm

Mixed Molecular Orientations Promote Charge Transport in Bulk Heterojunction Solar Cells

Journal:	*ChemComm*
Manuscript ID	CC-COM-03-2022-001234.R1
Article Type:	Communication

COMMUNICATION

Mixed Molecular Orientations Promote Charge Transport in Bulk Heterojunction Solar Cells

Pravini S. Fernando,[a] Detlef-M. Smilgies[b,c] and Jeffrey M. Mativetsky*[a,c]

Received 00th January 20xx,
Accepted 00th January 20xx

DOI: 10.1039/x0xx00000x

By systematically varying the molecular orientation of poly(3-hexylthiophene-2,5-diyl) (P3HT) in P3HT:fullerene bulk heterojunctions, we show that a mixed face-on and edge-on texture can be beneficial for out-of-plane charge flow in solution processed organic bulk heterojunction solar cells. These results implicate the need to balance in-plane and out-of-plane pathways for efficient charge percolation in bulk heterojunctions.

Solution processed organic solar cells (OSCs) offer a promising route towards lightweight, cost-effective, flexible, and optically tunable photovoltaics.[1,2] OSCs have shown superior performance under indoor and outdoor conditions, surpassing power conversion efficiencies (PCEs) of 31%[3] and 19%,[4] respectively. High performance OSCs employ the bulk heterojunction (BHJ) concept,[5] i.e., an interpenetrating nanoscale network of electron donating and electron accepting domains, to promote exciton dissociation. The morphological details of a BHJ, including the domain size, purity, crystallinity, etc,[2,6] strongly impact charge photogeneration, charge transport, and the PCE.

Molecular orientation is recognized as a key parameter affecting light absorption, exciton dissociation, charge transport, and energy level alignment.[7] For π-stacking molecules, a face-on orientation, with the molecular plane lying parallel to the substrate, enables efficient vertical charge transport within the molecular stacks.[8,9] On the other hand, an edge-on orientation, with the molecular plane standing upright with respect to the substrate, creates efficient lateral pathways in a film.[10] Efforts to promote out-of-plane charge transport in OSCs have therefore emphasized face-on molecular stacking as a desired structural feature within BHJ active layers,[8,11] while edge-on stacking is commonly seen as unintended and detrimental. In line with this thinking, numerous studies have noted charge carrier mobility and PCE gains caused by face-on molecular stacking in BHJ active layers .[12–14]

Although molecular orientations in organic electronic systems are commonly described in ways that imply the dominance of a single edge-on or face-on orientation, BHJ films can have a mixed face-on and edge-on texture.[15–17] Interestingly, recent studies that analyze the texture of BHJ films have indicated that increased face-on content does not always improve OSC performance. One study found that optimized P2TBR:IDIC BHJ films with a co-existing face-on and edge-on texture of the donor P2TBR had a higher PCE and fill factor than predominantly face-on oriented blend films.[16] It was also reported that a coexisting face-on/edge-on texture of donor molecules in the ternary blend DR3TSBDT:PTB7-Th:$PC_{71}BM$ led to improved hole transport and power conversion compared to highly face-on bicomponent PTB7-Th:$PC_{71}BM$.[17] A mixed face-on and edge on texture was also present in several other efficient BHJ OSC systems.[15,18,19]

These observations challenge the commonly held notion that a face-on orientation necessarily favors out-of-plane charge transport in BHJ devices and suggest instead that out-of-plane charge percolation is facilitated by the presence of both vertical and lateral charge transport pathways. Lateral pathways provided by an edge-on orientation can promote three-dimensional charge flow by helping holes circumvent acceptor domains in which hole transport is excluded, or by helping electrons avoid donor domains in which electron transport is excluded. This conclusion is supported by a recent study from our group that correlated in-plane π-stacking with out-of-plane hole mobility in a small molecule BHJ[20] and several studies that show signatures of three-dimensional charge percolation in BHJs.[21–23] The emerging picture reflects the fact that charge transport in BHJs is fundamentally different from that in single component films, since in BHJs, charge must navigate around excluded volumes.

While there is accumulating, albeit indirect evidence that in-plane pathways play an essential role in BHJs, directly assessing the impact of in-plane pathways on out-of-plane charge transport presents a technical challenge. In this study, we apply a recently introduced approach to quantify the contribution of lateral pathways to out-of-plane charge transport by measuring the effective current spreading area during conductive atomic force microscopy (C-AFM) in a vertical geometry.[24] By

[a] *Department of Physics, Applied Physics and Astronomy, Binghamton University, Binghamton, New York, 13902, United States. E-mail: jmativet@binghamton.edu*
[b] *Center of Advanced Microelectronics Manufacturing (CAMM), Binghamton University, Binghamton, New York, 13902, United States*
[c] *Materials Science and Engineering Program, Binghamton University, Binghamton, New York, 13902, United States*
Electronic Supplementary Information (ESI) available: [details of any supplementary information available should be included here]. See DOI: 10.1039/x0xx00000x

systematically varying the proportion of edge-on and face-on donor molecules in BHJ samples, we show that a mixed edge-on and face-on texture, and a balance of lateral and vertical transport channels, can facilitate out-of-plane charge transport. BHJ active layers were prepared comprising the polymer donor poly(3-hexylthiophene-2,5-diyl (P3HT) and the fullerene acceptor [6,6]-phenyl-C_{61}-butyric acid methyl ester ($PC_{61}BM$). The proportion of face-on and edge-on P3HT populations was tuned by varying the annealing temperature (see Supplementary Information for details).[25] As shown in Fig. 1a, the grazing-incidence wide-angle X-ray scattering (GIWAXS) pattern for a P3HT:$PC_{61}BM$ BHJ film annealed at 100 °C features peaks associated with both face-on and edge-on P3HT stacking. Edge-on P3HT stacking is evident from the distinct (100) lamellar peak at q_z = 0.38 Å $^{-1}$, higher order (200) and (300) reflections, and in-plane π–π stacking (010) peak at q_x=1.6 Å $^{-1}$. The out-of-plane π–π stacking (010) peak at q_z =1.6 Å $^{-1}$ and the (100) lamellar peak at q_x = 0.38 Å $^{-1}$ correspond to a face-on orientation of P3HT.

To obtain the population of edge-on, face-on, and isotopically-oriented P3HT, we analyzed the azimuthal dependence of the (100) lamellar peak at q = 0.38 Å $^{-1}$ of the (q_{xy},q_z) GIWAXS patterns (see Supplementary Information, Fig. S3). Since the detector plane only probes a slice of the three-dimensional reciprocal space, to quantify the oriented populations over the full reciprocal space, the scattering intensity along the azimuthal angle (χ) was adjusted by multiplying the integrated intensity by sin(χ).[26,27] Fig. 1b shows the corrected (100) intensity distribution for the 100 °C annealed P3HT:$PC_{61}BM$ blend. Intensities above the sin(χ) baseline at χ smaller than 45° were integrated to obtain the edge-on population, while intensities above the sin(χ) baseline at χ greater than 45° were integrated to obtain the face-on population. The isotropic contribution is given by integrating under the sin(χ) baseline.

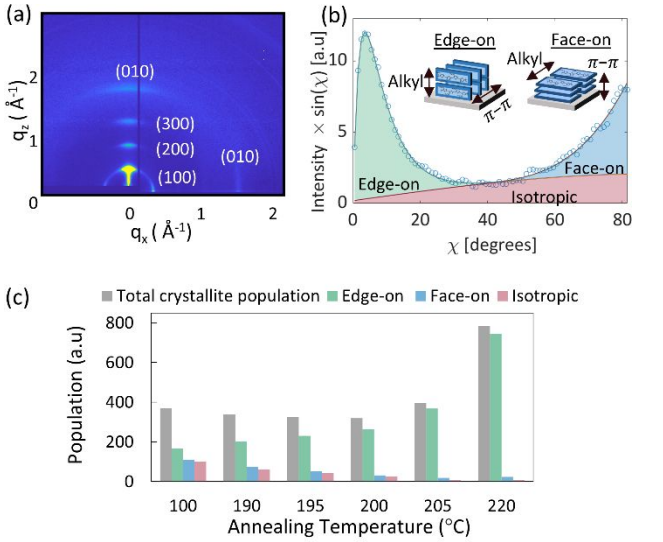

Fig.1 (a) GIWAXS pattern for a P3HT:PC61BM BHJ film annealed at 100 °C. (b) Azimuthal integration of the P3HT (100) peak along χ, corrected to account for the curvature of the Ewald sphere, with contributions from edge-on (green), face-on (blue), and isotropically oriented (pink) P3HT. (c) Total P3HT crystallite (gray), edge-on (green), face-on (blue) and isotropic (pink) population as a function of annealing temperature.

As shown in Fig. 1c, as the annealing temperature is increased, the P3HT molecules within the film increasingly favor an edge-on orientation, with the edge-on proportion growing from 44 % to 95 % over the measured annealing range. Correspondingly, the face-on and isotropic proportions decrease from 29 % to 3 % and 27 % to 1 %, respectively.

As shown in Fig. 1c, the overall P3HT crystallite population slightly decreases up to 200 °C. Therefore, the increase in edge-on fraction for films annealed up to 200 °C can be attributed to a reorientation of existing face-on and isotropic P3HT crystallites to an edge-on orientation. For films annealed above 205 °C, a sharp increase in total crystallite population is observed, while the increase in edge-on population is greater than the drop in face-on and isotropically oriented populations. Therefore, the increase in edge-on fraction is mainly due to the conversion of amorphous P3HT to edge-on P3HT crystallites, most likely due to heterogeneous crystallite nucleation at the substrate following melting and subsequent recrystallization during cooling.[25] The melting point of P3HT in the P3HT:$PC_{61}BM$ blends can be identified by the sudden increase in total crystallinity, between 200 °C and 205 °C.

To determine the effects of molecular orientation on charge transport, we used C-AFM to quantify the effective lateral current spreading radius and the average out-of-plane hole current for each film in a nitrogen environment. Fig. 2a shows a schematic of the C-AFM setup used for quantifying current spreading. Hole-only charge transport was achieved by using a high work function Au-coated C-AFM probe and a PEDOT:PSS hole transport layer. Au microelectrodes of known area were patterned onto the active layer and a C-AFM current map was recorded over sample regions that include both the bare film and the microelectrodes (Fig. 2b inset).[24] As shown in the current histogram Fig. 2b, the sharp peak at lower currents, centered at 0.16 nA, represents the current I_p through the uncoated BHJ film, whereas the broad peak centered at 87.4 nA represents the current I_m, when the probe is in contact with the micropatterned electrodes. The effective current spreading area A_{eff} during C-AFM can be obtained from $A_{eff} = (I_p/I_m)A_m$ where A_m is the microelectrode area[24]. It should be noted that the effective current spreading area during C-AFM depends on the active layer morphology, active layer thickness, and applied bias voltage.[28] By maintaining a constant film thickness and bias voltage, lateral current spreading can be used as a measure of a film's charge transport anisotropy.[24]

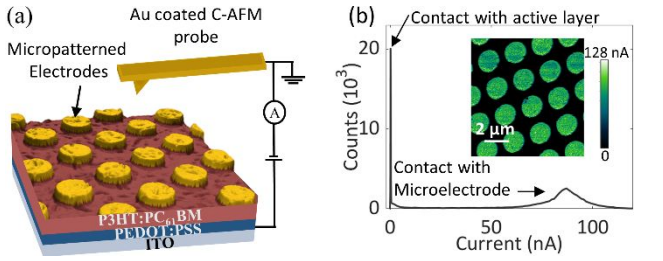

Fig. 2 (a) C-AFM setup used for quantifying lateral current spreading during C-AFM. (b) A current map (inset) and corresponding current histogram for a P3HT:$PC_{61}BM$ BHJ film annealed at 220°C.

Fig. 3 shows the variation of lateral current spreading radius, average out-of-plane hole current, and edge-on to face-on ratio with annealing temperature. At 100 °C, the P3HT:PC_{61}BM BHJ film has comparable edge-on and face-on populations, with a ratio of 1.5, whereas at 220 °C, the film is predominantly edge-on, with an edge-on to face-on ratio of 32. The current spreading radius closely correlates with the edge-on to face-on ratio, with a coefficient of determination of 0.967 (see Supplementary Information, Fig. S4), illustrating the strong influence of edge-on stacking on lateral charge flow. Interestingly, the average hole current, obtained by averaging all pixels in C-AFM hole current maps (see Supplementary Information, Fig. S5), initially increases, reaching a maximum at 195 °C, and then decreases with annealed temperature. In other words, the maximum hole current was not observed for the BHJ blend with the highest face-on population. Instead, an edge-on to face-on ratio of 4.4 (annealed at 195 °C) led to a 31 % higher out-of-plane hole current compared to film with an edge-on to face-on ratio of 1.5 (annealed at 100 °C). Films with predominantly edge-on P3HT led to extensive lateral spreading, but inefficient out-of-plane charge transport. A similar hole current trend is also observed at other bias voltages (see Supplementary Information, Fig. S6).

This result shows that an increase in face-on population does not necessarily enhance out-of-plane charge transport in a BHJ. Fig. 4a illustrates the case of a film with a predominantly face-on donor molecule orientation. Although the face-on donor stacks present efficient vertical pathways for holes, a lack of efficient lateral pathways forces holes to take inefficient routes to circumvent the acceptor regions. On the other hand, with a balance of face-on and edge-on orientations, as illustrated in Fig. 4b, efficient vertical and lateral pathways are available to allow holes to effectively bypass acceptor domains. A predominantly edge-on orientation, depicted in Fig. 4c, results in greater lateral spreading, but a lower out-of-plane current due to the lack of efficient vertical charge transport channels. In addition to molecular orientation, factors such as crystallite population and crystallite size can also influence charge transport.[29]

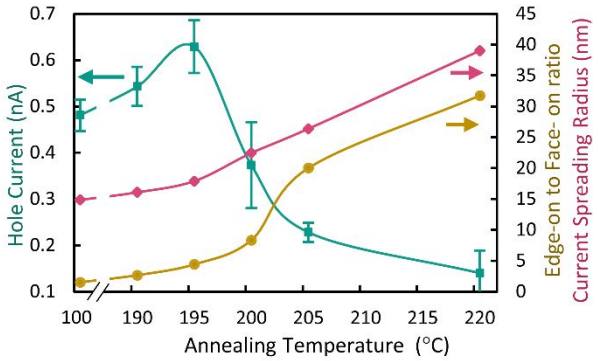

Fig. 3 Average hole current (green), edge-on: face-on ratio (yellow), and current spreading radius (pink) as a function of P3HT:PC_{61}BM annealing temperature. The left y-scale represents the average hole current and the right y-scale represents both the edge-on: face-on ratio and current spreading radius (in nm). The curves are included as a visual aid to observe overall trends.

As discussed earlier (and shown in Fig. 1c), for films annealed up to 200°C, we observed a slight drop in the total P3HT crystallite population; therefore, the improvement in hole transport between 100 °C to 195 °C cannot be attributed to an increase in crystallinity.

To assess the effect of thermal annealing on crystallite size, the P3HT average grain size was determined from the radial full width at half maximum of the out-of-plane (100) peak, using the Scherrer equation. As shown in the Supplementary Information (Fig. S2), a gradual increase in average grain size was observed with temperature. The increase in average grain size from 190 °C to 195 °C amounts to only 5%, whereas the edge-on:face-on ratio increases by 66%, suggesting that the change in molecular orientation played a stronger role in the observed hole transport increase at 195 °C. In support of the dominant role played by molecular orientation, above 200 °C, the crystallite population and average grain size both increase (see Fig. 1c and Supplementary Information Fig. S2), which should promote charge transport; instead, however, the out-of-plane current continuously decreases as the P3HT becomes increasingly edge-on and lateral pathways are increasingly favored.

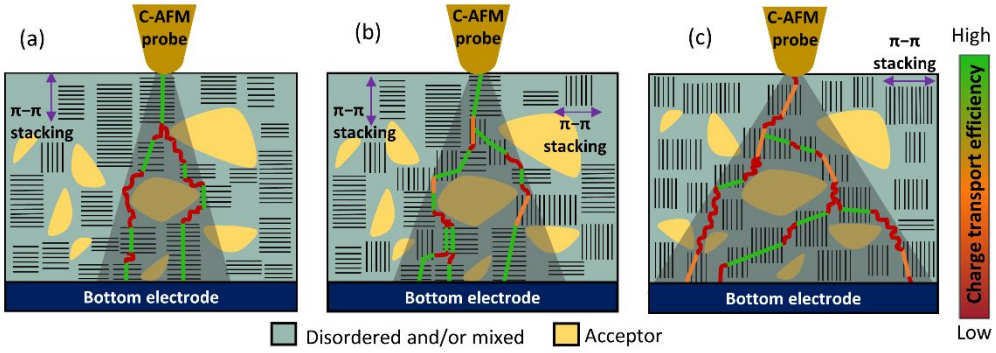

Fig. 4 Illustration of hole transport through a BHJ active layer (a) with predominantly face-on oriented donor domains, (b) with a balanced mixture of face-on and edge-on donor domains, and (c) with predominantly edge-on oriented donor domains. The black parallel lines represent the orientation of the donor molecules. The green, orange, and red line segments represent hole transport pathways with efficient, moderately efficient, and inefficient hole transport, respectively. Transport is most efficient along π-π stacks, less efficient when transport is along other crystallographic directions, and poor within disordered or finely mixed donor-acceptor regions. The shaded regions represent the hole current spreading range. The spreading broadens as the edge-on donor population increases.

In summary, to evaluate the effect of molecular orientation on out-of-plane charge transport in BHJs, we varied the proportion of face-on and edge-on P3HT populations in P3HT:$PC_{61}BM$ films and quantified lateral current spreading and out-of-plane hole current during C-AFM. Rather than observing the highest out-of-plane hole current for films with the highest face-on P3HT population, we noted the highest out-of-plane current when there was an intermediate mixture of face-on and edge-on populations. For predominantly edge-on films, out-of-plane charge transport was inefficient due a lack of vertical transport channels. In view of these results, we propose that charge collection in BHJ OSCs should be promoted by balancing the availability of in-plane and out-of-plane pathways, through a combined face-on and edge-on texture. It should be noted that other BHJ systems may require a different balance of edge-on and face-on proportions, depending on system details that influence the anisotropy of intermolecular charge transfer (e.g., conjugated core structure, choice of solubilizing chain, molecular packing motif, molecular stacking distance).[30,31] The presented study lays the groundwork for probing the effects of molecular orientation on charge transport anisotropy in new OSC materials, for insight into the orientational texture needed for efficient charge transport and collection.

This work was supported by the National Science Foundation (CAREER award DMR-1555028) and Binghamton University's Smart Energy Transdisciplinary Area of Excellence. This research also used resources of the Complex Materials Scattering (CMS-11-BM) beamline of the National Synchrotron Light Source II, a U.S. Department of Energy (DOE) Office of Science user Facility operated for the DOE Office of Science by Brookhaven National Laboratory under Contract No. DE-SC0012704. We are indebted to Ruipeng Li for his expertise and for collecting the scattering data at the CMS beamline under COVID restrictions.

Notes and references

1 L. Meng, Y. Zhang, X. Wan, C. Li, X. Zhang, Y. Wang, X. Ke, Z. Xiao, L. Ding, R. Xia, H.-L. Yip, Y. Cao and Y. Chen, *Science* ., 2018, **361**, 1094–1098.

2 A. M. Haruk and J. M. Mativetsky, *Int. J. Mol. Sci.*, 2015, **16**, 13381–13406.

3 L.-K. Ma, Y. Chen, P. C. Y. Chow, G. Zhang, J. Huang, C. Ma, J. Zhang, H. Yin, A. M. Hong Cheung, K. S. Wong, S. K. So and H. Yan, *Joule*, 2020, **4**, 1486–1500.

4 Y. Cui, Y. Xu, H. Yao, P. Bi, L. Hong, J. Zhang, Y. Zu, T. Zhang, J. Qin, J. Ren, Z. Chen, C. He, X. Hao, Z. Wei and J. Hou, *Adv. Mater.*, 2021, **33**, 2102420.

5 Q. Liu, Y. Jiang, K. Jin, J. Qin, J. Xu, W. Li, J. Xiong, J. Liu, Z. Xiao, K. Sun, S. Yang, X. Zhang and L. Ding, *Sci. Bull.*, 2020, **65**, 272–275.

6 F. Zhao, C. Wang and X. Zhan, *Adv. Energy Mater.*, 2018, **8**, 1703147.

7 B. P. Rand, D. Cheyns, K. Vasseur, N. C. Giebink, S. Mothy, Y. Yi, V. Coropceanu, D. Beljonne, J. Cornil, J.-L. Brédas and J. Genoe, *Adv. Funct. Mater.*, 2012, **22**, 2987–2995.

8 J. M. Mativetsky, H. Wang, S. S. Lee, L. Whittaker-Brooks and Y.-L. Loo, *Chem. Commun.*, 2014, **50**, 5319–5321.

9 S. Chae, A. Yi, H. H. Lee, J. Choi and H. J. Kim, *J. Mater. Chem. C*, 2018, **6**, 9374–9382.

10 T. Ghosh, S. Nagasawa, N. Raveendran, V. Darshan, A. Saeki and V. C. Nair, *Chem. – An Asian J.*, 2019, **14**, 963–967.

11 J. A. Love, I. Nagao, Y. Huang, M. Kuik, V. Gupta, C. J. Takacs, J. E. Coughlin, L. Qi, T. S. van der Poll, E. J. Kramer, A. J. Heeger, T.-Q. Nguyen and G. C. Bazan, *J. Am. Chem. Soc.*, 2014, **136**, 3597–3606.

12 Q. Zhao, X. Yu, Z. Xie, J. Liu and Y. Han, *Org. Electron.*, 2020, **77**, 105512.

13 J. Zhao, Y. Li, G. Yang, K. Jiang, H. Lin, H. Ade, W. Ma and H. Yan, *Nat. Energy*, 2016, **1**, 15027.

14 W. Li, S. Albrecht, L. Yang, S. Roland, J. R. Tumbleston, T. McAfee, L. Yan, M. A. Kelly, H. Ade, D. Neher and W. You, *J. Am. Chem. Soc.*, 2014, **136**, 15566–15576.

15 V. Vohra, K. Kawashima, T. Kakara, T. Koganezawa, I. Osaka, K. Takimiya and H. Murata, *Nat. Photonics*, 2015, **9**, 403–408.

16 X. Li, Y. Wang, Q. Zhu, X. Guo, W. Ma, X. Ou, M. Zhang and Y. Li, *J. Mater. Chem. A*, 2019, **7**, 3682–3690.

17 T. Kumari, S. M. Lee, S.-H. Kang, S. Chen and C. Yang, *Energy Environ. Sci.*, 2017, **10**, 258–265.

18 L. Yang, S. Zhang, C. He, J. Zhang, H. Yao, Y. Yang, Y. Zhang, W. Zhao and J. Hou, *J. Am. Chem. Soc.*, 2017, **139**, 1958–1966.

19 S. Badgujar, C. E. Song, S. Oh, W. S. Shin, S.-J. Moon, J.-C. Lee, I. H. Jung and S. K. Lee, *J. Mater. Chem. A*, 2016, **4**, 16335–16340.

20 J. S. Mehta and J. M. Mativetsky, *ACS Appl. Energy Mater.*, 2018, **1**, 5656–5662.

21 J. D. Roehling, K. J. Batenburg, F. B. Swain, A. J. Moulé and I. Arslan, *Adv. Funct. Mater.*, 2013, **23**, 2115–2122.

22 K. Vakhshouri, D. R. Kozub, C. Wang, A. Salleo and E. D. Gomez, *Phys. Rev. Lett.*, 2012, **108**, 26601.

23 S. van Bavel, E. Sourty, G. de With, S. Veenstra and J. Loos, *J. Mater. Chem.*, 2009, **19**, 5388–5393.

24 P. S. Fernando, J. S. Mehta, D. M. Smilgies and J. M. Mativetsky, submitted.

25 E. Verploegen, R. Mondal, C. J. Bettinger, S. Sok, M. F. Toney and Z. Bao, *Adv. Funct. Mater.*, 2010, **20**, 3519–3529.

26 J. L. Baker, L. H. Jimison, S. Mannsfeld, S. Volkman, S. Yin, V. Subramanian, A. Salleo, A. P. Alivisatos and M. F. Toney, *Langmuir*, 2010, **26**, 9146–9151.

27 F. Li, K. G. Yager, N. M. Dawson, Y.-B. Jiang, K. J. Malloy and Y. Qin, *Polym. Chem.*, 2015, **6**, 721–731.

28 H. Qiu, X. Dong, J. H. Shim, J. Cho and J. M. Mativetsky, *Appl. Phys. Lett.*, 2018, **112**, 263102.

29 A. L. Ayzner, D. D. Wanger, C. J. Tassone, S. H. Tolbert and B. J. Schwartz, *J. Phys. Chem. C*, 2008, **112**, 18711–18716.

30 Y. Olivier, V. Lemaur, J. L. Brédas and J. Cornil, *J. Phys. Chem. A*, 2006, **110**, 6356–6364.

31 Y. Geng, S.-X. Wu, H.-B. Li, X.-D. Tang, Y. Wu, Z.-M. Su and Y. Liao, *J. Mater. Chem.*, 2011, **21**, 15558–15566.